Supporting Information

S.1. Supporting Information - Results

Coupling to the analysis in Section 3.1.1, relative pressure traces for two selected sections (right ICA, and right ICA-MCA) spatiotemporal samplings (dx = 1.0mm, dt = 40 ms, and dx = 0.5mm, dt = 40 ms) are provided in Supporting Information Figure S.1

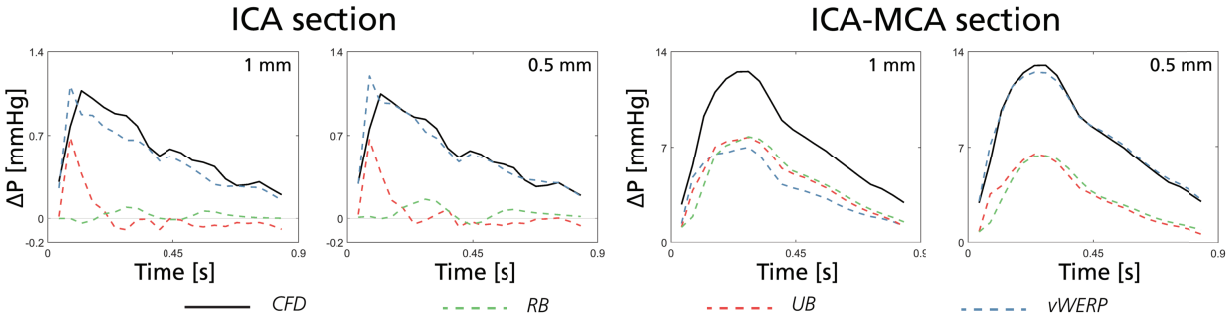

Supporting Information Figure S.1: Estimated relative pressures through the right ICA (left) and the right ICA-MCA section (right) in Subject 1. For both sections, results are shown for $dx = 1$ mm and 0.5 mm, with dt = 40 ms in both instances. In each graph, relative pressure estimates are given for RB (green dashed), UB (red dashed), νWERP (blue dashed), and true estimate given by voxelized equivalents of the CFD pressure field generated at the identical spatiotemporal sampling (black solid).

Furthermore, coupling to the analysis in Section 3.2, linear regression plots for $dx = 1.1$ vs. 0.8 mm are provided for all different evaluated methods, as well as for corresponding *in-silico* data, in Supporting Information Figure S.2.

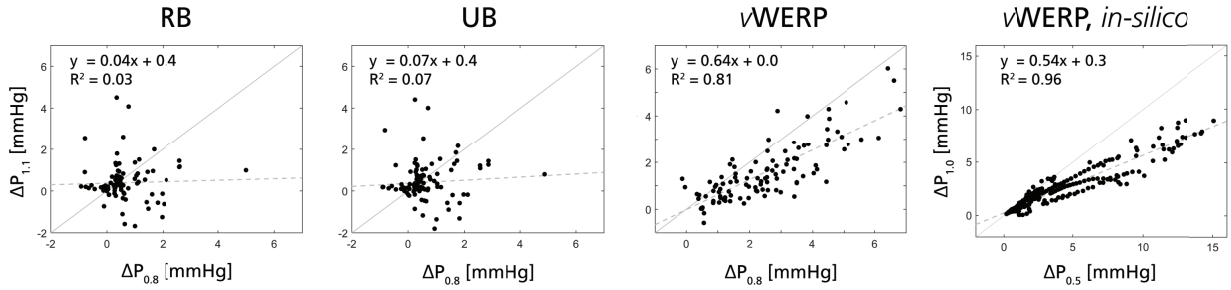

Supporting Information Figure S.2: Linear regression plots, comparing relative pressure estimates obtained at $dx = 1.1$ vs. 0.8 mm using RB, UB, and νWERP, respectively. For reference, νWERP results at $dx = 1.0$ vs. 0.5 mm from the *in-silico* tests (Section 3.1) are shown at the far right.

S.2. Supporting Information - Full Euler formulation and Unsteady Bernoulli

As noted in Sections 2.1 and 4.1.2, UB is based on the assumption that the utilized integration line $\mathbf{p}(s)$ follows a physiological streamline, for which the conversion from Eq. 4 to 5 holds true. In practice, selecting a physiological streamline is however cumbersome. and is often replaced by a user-defined integration line. Importantly, this choice is not

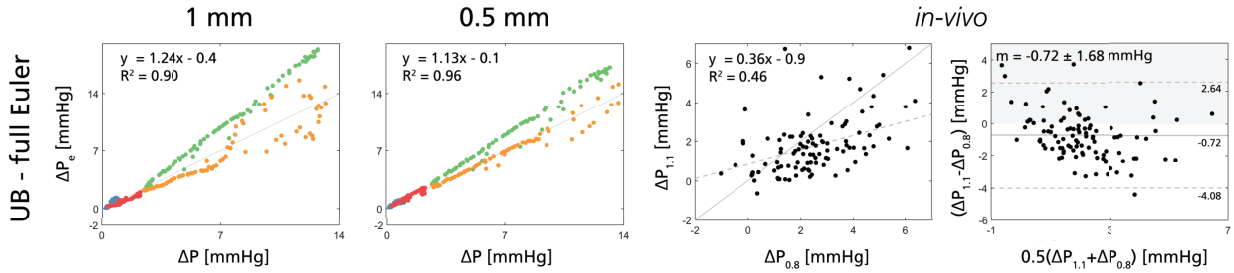

Supporting Information Figure S.3: Results from both the *in-silico* (spatiotemporal analysis from Section 2.2.2, shown for $dx = 1.0$ and 0.5 mm, cf. Figure 4) and *in-vivo* analysis (linear regression and Bland-Altman plot for $dx = 1.1$ vs. 0.8 mm, cf. Figure 8), utilizing a full Euler UB expression, including $\nabla \mathbf{v}$ in the expression of the advective term.

only practical, but works well if assessing predominantly unidirectional flow. If assessing flow with dominant spatial gradients, however, the chosen integration path might no longer validly represent that of a physiological streamline.

To circumvent dependency on utilized integration line, one can instead revert back to the full Euler form given in Eq. 4. Here, the integration path is no longer restricted to that of a physiological streamline, however, derivation requires access to the gradient of the velocity field (as permitted by 4D Flow MRI). Herein, it should be stressed that this formulation represents a non-conventional usage of UB where access to $\nabla \mathbf{v}$ is normally *not* provided (such as when using Doppler echocardiography). Nevertheless, if indeed invoking a full Euler UB expression (Eq. 4), results improve distinctly as shown in Supporting Information Figure S.3, showing exemplifying output from the spatiotemporal analysis (cf. Section 3.1.1) and the *in-vivo* analysis (cf. Section 3.2), respectively. Comparing the standard UB formulation over the spatiotemporal analysis, average d_f decreases to 25.9%, and if focusing on comparably high resolutions ($dt \leq 40$ ms, $dx \leq 0.75$ mm) d_f goes down to 19.8%. Likewise, in the *in-vivo* data correlations between $dx = 1.1$ and 0.8 mm improve slightly, although not to the level observed with νWERP.

Accurate output can thus in principle be achieved if invoking a full Euler form of the UB. However, it should again be stressed that this does *not* represent the clinical standard use of UB, and the results instead highlight practical obstacles associated with using UB in complex vascular settings.